Brief Communication

MOLECULAR METABOLISM

Metabolic remodeling of dystrophic skeletal muscle reveals biological roles for dystrophin and utrophin in adaptation and plasticity

Justin P. Hardee [1], Karen J.B. Martins [1], Paula M. Miotto [2], James G. Ryall [1], Stefan M. Gehrig [1], Boris Reljic [3], Timur Naim [1], Jin D. Chung [1], Jen Trieu [1], Kristy Swiderski [1], Ashleigh M. Philp [4,5], Andrew Philp [4,5], Matthew J. Watt [2], David A. Stroud [3], Rene Koopman [1], Gregory R. Steinberg [6], Gordon S. Lynch [1,*]

ABSTRACT

Objectives: Preferential damage to fast, glycolytic myofibers is common in many muscle-wasting diseases, including Duchenne muscular dystrophy (DMD). Promoting an oxidative phenotype could protect muscles from damage and ameliorate the dystrophic pathology with therapeutic relevance, but developing efficacious strategies requires understanding currently unknown biological roles for dystrophin and utrophin in dystrophic muscle adaptation and plasticity.

Methods: Combining whole transcriptome RNA sequencing and mitochondrial proteomics with assessments of metabolic and contractile function, we investigated the roles of dystrophin and utrophin in fast-to-slow muscle remodeling with low-frequency electrical stimulation (LFS, 10 Hz, 12 h/d, 7 d/wk, 28 d) in *mdx* (dystrophin null) and *dko* (dystrophin/utrophin null) mice, two established preclinical models of DMD.

Results: Novel biological roles in adaptation were demonstrated by impaired transcriptional activation of estrogen-related receptor alpha-responsive genes supporting oxidative phosphorylation in dystrophic muscles. Further, utrophin expression in dystrophic muscles was required for LFS-induced remodeling of mitochondrial respiratory chain complexes, enhanced fiber respiration, and conferred protection from eccentric contraction-mediated damage.

Conclusions: These findings reveal novel roles for dystrophin and utrophin during LFS-induced metabolic remodeling of dystrophic muscle and highlight the therapeutic potential of LFS to ameliorate the dystrophic pathology and protect from contraction-induced injury with important implications for DMD and related muscle disorders.

Keywords Muscular dystrophy; Muscle adaptation; Dystrophin; Utrophin; Oxidative metabolism

1. INTRODUCTION

In Duchenne muscular dystrophy (DMD) and well-characterized murine models of the disease linked to the genetic loss of the protein dystrophin, fast muscle fibers are more susceptible to contraction-mediated damage and pathological progression than slow muscle fibers, which are resistant to injury and relatively spared [1]. The resistance of oxidative muscle fibers to injury and pathology in preclinical models is attributed, in part, to their higher expression of utrophin-A compared with glycolytic fibers [2,3], and overexpression of utrophin can ameliorate the dystrophic phenotype in dystrophin-deficient *mdx* mice [4–6]. Strategies promoting an oxidative phenotype also increase utrophin-A expression [7,8], highlighting the therapeutic potential of muscle plasticity to mitigate the dystrophic pathology. Developing strategies along these lines requires an improved understanding of the biological roles of dystrophin and utrophin in dystrophic muscle adaptation and plasticity, but to date, these roles have not been fully elucidated.

Muscles of DMD patients and mouse models of dystrophy have impaired oxidative phosphorylation and mitochondrial function [9–11], which contribute to the disease etiology. Chronic low-frequency electrical stimulation (LFS) has improved understanding of the adaptive and metabolic plasticity of skeletal muscle [12,13], and in preliminary trials, this approach has shown potential for improving muscle strength in DMD patients [14–17] and in mouse models of muscular dystrophy [18–20]. A mechanistic understanding of the biological roles of dystrophin and utrophin in these beneficial adaptations remains elusive but is essential if LFS is to be optimized as an adjunct therapy for DMD and related disorders. Although a cure for DMD may eventually come from corrective gene

[1]Centre for Muscle Research, Department of Anatomy and Physiology, The University of Melbourne, Melbourne, Victoria, 3010, Australia [2]Department of Physiology, The University of Melbourne, Melbourne, Victoria, 3010, Australia [3]Department of Biochemistry and Molecular Biology, The Bio21 Institute, The University of Melbourne, Melbourne, 3010, Victoria, Australia [4]Garvan Institute of Medical Research, Sydney, New South Wales, 2010, Australia [5]St Vincent's Clinical School, UNSW Medicine, UNSW Sydney, Sydney, 2010, New South Wales, Australia [6]Division of Endocrinology and Metabolism, Department of Medicine, the Department of Biochemistry and Biomedical Sciences and the Center for Metabolism, Obesity, and Diabetes Research, McMaster University, Hamilton, ON, L8S 4L8, Canada

*Corresponding author. Centre for Muscle Research, Department of Anatomy and Physiology, The University of Melbourne, Melbourne, Victoria, 3010, Australia. E-mail: gsl@unimelb.edu.au (G.S. Lynch).

Received November 23, 2020 • Revision received December 21, 2020 • Accepted December 22, 2020 • Available online 24 December 2020

https://doi.org/10.1016/j.molmet.2020.101157

therapies, limitations of delivery systems, gene-carrying capacity, dissemination efficiency, expression persistence, and immunological tolerance all pose significant obstacles for clinical application. There remains an urgent and unmet clinical need for therapies that can ameliorate the pathology, preserve and protect muscles from damage, and ultimately serve as adjuvant therapies for any gene- or cell-based approach. To resolve the shortfall in understanding how dystrophic muscles could adapt optimally to LFS, the present study combined whole transcriptome RNA sequencing and mitochondrial proteomics with assessments of metabolic and contractile function in *mdx* (dystrophin null) and *dko* (dystrophin/utrophin null) mice during fast-to-slow muscle remodeling with LFS. We uncovered novel biological roles for dystrophin and utrophin in the functional remodeling of dystrophic muscle with LFS and the adaptive mechanisms that can confer protection against contraction-induced injury, with therapeutic significance for DMD and related disorders.

2. MATERIALS AND METHODS

2.1. Animals

Male C57BL/10ScSn (BL/10) and dystrophin deficient (*mdx*) mice were obtained from the Animal Resources Center (Canning Vale, WA, Australia) at 3 weeks of age. Age-matched, male mice lacking dystrophin and utrophin (*dko*) were bred in the Biological Research Facility at The University of Melbourne. The *mdx* mice exhibit a mild dystrophic phenotype, highlighted by fiber necrosis from 3 to 6 weeks of age and then a stable degeneration/regeneration phase that persists into late life [21]. In contrast, the *dko* mice exhibit a severe and progressive muscular dystrophy that more closely mimics the phenotypic characteristics of DMD, with premature death occurring between 6 and 20 weeks of age [22,23]. Chronic low-frequency electrical stimulation (LFS) was performed between 5 and 9 weeks of age. All mice were housed under a 12-hour light/dark cycle and provided access to drinking water and standard chow *ad libitum*. At the time of death, excised tissues were weighed and frozen in liquid nitrogen or processed for downstream analyses. All experiments were approved by the Animal Ethics Committee of The University of Melbourne (AEC 1212507, 1613961) and conducted in accordance with the Australian code of practice for the care and use of animals for scientific purposes as stipulated by the National Health and Medical Research Council (Australia).

2.2. Surgical implantation of electrodes and chronic LFS

At 4 weeks of age, wireless bipolar electrodes were surgically implanted dorsally within the interscapular region of anesthetized mice (75 mg/kg body wt. of ketamine; 10 mg/kg body wt. of xylazine), while the stimulating electrode wires were sutured around the sciatic nerve proximal to its point of trifurcation. Following complete recovery (3–7 days), chronic LFS (10 Hz, impulse width 380 μs, 12 h/d) was performed daily for 28 days during the light cycle in a custom-built stimulator to allow muscular contractions in conscious, free-moving animals. Mice were returned to their home cage during the dark cycle and had access to food and water *ad libitum*.

2.3. Histology, immunohistochemistry, and citrate synthase activity

Tibialis anterior (TA) muscles were embedded in optimal cutting temperature compound, and frozen in isopentane cooled in liquid nitrogen. Serial sections (8 μm) were mounted on uncoated, pre-cleaned glass slides. Sections were stained and analyzed as described previously [23–25].

2.4. RNA extraction, sequencing, and bioinformatics

Whole transcriptome sequencing (mRNA-Seq) was completed as described previously [26–29]. Gene ontology and transcriptional factor enrichment were analyzed using the online bioinformatics resource DAVID (National Institute of Allergy and Infectious Diseases, NIH) [30] and The Molecular Signatures Database (MSigDB) [31,32].

2.5. High-resolution respirometry in permeabilized muscle fibers

Mitochondrial respiration measurements were performed in permeabilized extensor digitorum longus (EDL) muscle fibers using high-resolution respirometry (Oxygraph-2K; Oroboros) at 37 °C, as described previously [33,34]. Complex I-supported respiration was determined by titrating adenosine diphosphate (ADP, 100–8,000 μM; A5285; Sigma) until a plateau was achieved in the presence of saturating pyruvate (5 mM; P2256; Sigma) and malate (2 mM; 46940; Sigma). Subsequently, glutamate (10 mM; G1626; Sigma) and succinate (10 mM; S2378; Sigma) were added to determine maximal complex I- and complex II-supported respiration, respectively. Cytochrome c (10 mM; C7752; Sigma) was added in all experiments to ensure mitochondrial integrity, demonstrated by $<$10% change in respiration.

2.6. Mitochondrial isolation and blue native polyacrylamide gel electrophoresis (BN-PAGE)

Analysis of gastrocnemius (GAS) mitochondrial respiratory chain supercomplexes was conducted using BN-PAGE [35]. In-gel activity of complex I was determined by incubating the gels in 5 mM of Tris–HCl (pH 7.4), 0.1 mg/ml of β-nicotinamide adenine dinucleotide (NADH; N4505; Sigma), and 2.5 mg/ml nitrotetrazolium blue chloride (NBT; N6876; Sigma). Gels were then stained for total protein using Coomassie Blue (LC6065; Invitrogen).

2.7. Mitochondrial proteomics

Proteomic analysis of crude mitochondrial protein from GAS muscles was performed as previously described with slight modifications [36–38]. Briefly, pre-normalized protein pellets were solubilized and digested into tryptic peptides and labeled (6-plex TMT; 90061; ThermoFisher Scientific). Pooled samples were fractionated, dried, and reconstituted. Liquid chromatography (LC) coupled tandem mass spectrometry (MS/MS) was carried out on an Orbitrap Lumos mass spectrometer (ThermoFisher Scientific) with a nanoESI interface in conjunction with an Ultimate 3000 RSLC nanoHPLC (Dionex Ultimate 3000. False discovery rates (FDR) were determined through the target-decoy approach set to 1% for both peptides and proteins. The proteinGroups.txt output from the search was processed in Perseus (version 1.6.2.2) [39]. Log2-transformed TMT reporter intensity corrected values were grouped into wild-type, *mdx,* and *dko* groups consisting of three replicates each. Identifications were filtered to include 100% valid values across all samples. Annotations for proteins present in the Mitocarta2.0 dataset were added through matching by gene name and rows filtered to include only mitochondrial entries [40]. A two-sided t-test with significance determined by permutation-based FDR statistics (FDR 5%, S = 1) was performed to identify differentially expressed proteins.

2.8. Immunoblotting

GAS muscles were homogenized, and western blotting was performed as described previously [41]. The following antibodies were used: anti-SIRT1 (#9475), anti-SIRT3 (#5490), and anti-rabbit (#7074) antibodies (Cell Signaling). Values were then normalized by total protein stain and expressed relative to muscles from BL/10 sham mice.

2.9. Assessment of muscle function *in situ*

Contractile function of TA muscles *in situ* were performed as described previously [42]. In brief, maximum isometric tetanic force was determined from the plateau of a complete frequency—force relationship. Assessment of contraction-induced injury was determined by maximally stimulating muscles for an isometric contraction and then lengthened at a velocity of two fiber lengths per second at progressively greater magnitudes of stretch. Force deficits were expressed as a percentage of maximum isometric force.

2.10. Statistical analysis

Data are presented as mean ± standard error of the mean unless otherwise noted. Statistical values were calculated by either a one-way analysis of variance (ANOVA), two-way ANOVA, or Student's t-test when appropriate. A P value of <0.05 was considered statistically significant. GraphPad Prism 8 software (GraphPad, San Diego, CA) and Microsoft Excel (Microsoft, Redmond, WA) were used for data processing.

3. RESULTS AND DISCUSSION

Chronic LFS (10 Hz) of the sciatic nerve provides an impulse pattern similar to that of a slow motor neuron which induces profound fast-to-slow phenotype remodeling of skeletal muscle [13]. We first determined the role of dystrophin and utrophin in dystrophic muscle adaptations to LFS (12 h/d, 7 d/wk, 28 d). Stimulated TA muscles of wild-type mice were smaller and deep red in color compared with unstimulated (pale) control muscles (Figure S1A,B). Stimulated TA muscles from *mdx* and *dko* mice were similarly smaller and deep red in color, with evidence of reduced fibrosis and calcium deposition, compared with unstimulated muscles (Figure S1A,B). Myofiber succinate dehydrogenase (SDH) activity in muscles of wild-type mice was increased by LFS (Figure 1A; S1C), and this adaptive response was not altered in muscles of *mdx* and *dko* mice (Figure 1A; S1C). Furthermore, the remodeling to a more oxidative phenotype involving reductions in myofiber diameter and variance coefficient was not altered by the loss of dystrophin or utrophin in dystrophic muscles (Figure S1D,E). In wild-type mice, LFS increased the abundance of type IIA fibers, CD31+ endothelial cells, and Pax7+ stem (satellite) cells (Figure 1A; S1F—H). While increases in the percentage of type IIA fibers and number of CD31+ endothelial cells were also observed in muscles of *mdx* and *dko* mice (Figure 1A; S1F,G), the number of Pax7+ stem (satellite) cells was unaltered by LFS in muscles of *dko* mice (Figure 1A; S1H). Collectively, these findings demonstrate that morphological properties of dystrophic muscles retain adaptive potential, while loss of dystrophin and utrophin in dystrophic muscles impedes the induction of muscle stem (satellite) cells with LFS.

To elucidate the role of dystrophin and utrophin in dystrophic muscle adaptation and plasticity, we performed whole transcriptome RNA sequencing after LFS. In extensor digitorum longus (EDL) muscles of wild-type mice, we identified a total of 855 genes [false discovery rate (FDR) $<$ 0.05] that were differentially expressed after LFS (Figure S2A,D). In contrast, the overall abundance of differentially expressed genes was lower in muscles of *mdx* and *dko* mice after LFS (*mdx*: 472; *dko*: 257; Figure S2B-D). Thus, dystrophin deficiency influenced 45% of differentially expressed genes by LFS in the muscles of wild-type mice, whereas utrophin-deficiency influenced 46% of differentially expressed genes by LFS in muscles of *mdx* mice. Similar observations were also noted when examining the number of genes unique to each group (Figure S2E). Functional annotation and gene ontology (GO) term analyses revealed transcriptional reprogramming toward a slow muscle phenotype, evident from the enrichment of upregulated genes in terms related to oxidation-reduction, fatty acid and lipid metabolism, carbon metabolism, oxidative phosphorylation, and mitochondria in muscles of wild-type mice (Figure S2F). While many of these terms were enriched in genes found upregulated by LFS in muscles of *mdx* and *dko* mice, the enrichment of these annotated genes was less significant (Figure S2F). Interestingly, while oxidative phosphorylation and the respiratory chain were significantly enriched in wild-type mice after LFS (Figure S2F), this was not observed in muscles of *mdx* and *dko* mice. In support of a shift toward a more oxidative phenotype, genes involved in the tricarboxylic acid (TCA) cycle, fatty acid metabolism, and β-oxidation were increased by LFS, while carbohydrate and glycogen metabolic processes were decreased by LFS (Figure 1B). Transgenic overexpression of nuclear receptors and coactivators that regulate the slow muscle phenotype have improved our understanding of metabolic and functional remodeling in dystrophic skeletal muscle, but the biological roles of utrophin expression in these adaptive responses has not been tested rigorously. Transcription factor enrichment analysis identified V$ERR1_Q2, which matches the mouse homolog of human estrogen-related receptor alpha (*Esrra* in mice), as the top transcription factor regulating genes increased by LFS in muscles of wild-type mice (Figure S2G), which was greatly reduced in muscles of *mdx* and *dko* mice. In line with this, the total number of *Esrra* target genes increased by LFS was lower and more variable in muscles of *mdx* and *dko* mice (Figure 1C; S2H), which may be attributed to the dysregulation of estrogen-related receptor isoform expression (Figure 1D). Overall, these data demonstrate that while LFS is sufficient to drive morphological adaptations in muscles of dystrophic mice, transcriptional activation after LFS is impaired by the loss of dystrophin and utrophin in dystrophic muscles.

Since the enrichment of terms related to oxidative phosphorylation and respiratory chain were lacking in genes differentially expressed by LFS in muscles of *mdx* and *dko* mice compared with wild-type mice (Figure 1B; S2F), we further explored the role of dystrophin and utrophin in the remodeling of mitochondrial structure and function. Strikingly, genes involved in oxidative phosphorylation and mitochondrial ribosomes were increased by LFS in muscles of wild-type mice, whereas this adaptive response was blunted in muscles of *mdx* and *dko* mice (Figure 2A). Interestingly, dysregulation of electron transfer flavoproteins was not observed in muscles of *mdx* and *dko* mice (Figure 2A), consistent with improved gene expression related to fatty acid metabolism and β-oxidation with LFS (Figure 1B). Together, these data demonstrate that the loss of dystrophin and utrophin in dystrophic muscles impairs transcriptional remodeling of oxidative phosphorylation after LFS.

Mitochondria are highly dynamic organelles that adapt to mechanical and environmental cues to maintain cellular energy homeostasis, but a role for dystrophin and utrophin in this remodeling process had not been fully described. To assess the functional consequences of reduced transcriptional remodeling to LFS, we performed high-resolution respirometry on permeabilized EDL muscle fiber bundles. Complex I-supported leak respiration (CI_L; pyruvate + malate) was increased with LFS in muscles of wild-type mice, but this adaptive response was attenuated in muscles of *mdx* and *dko* mice (Figure 2B). Complex - supported respiration (CI_P; pyruvate + malate + ADP) was increased across all ADP concentrations (100—8,000 μM) with LFS in muscles of wild-type mice (Figure 2E), whereas it was attenuated in muscles of *mdx* mice (Figure 2F) and completely abrogated in muscles of *dko* mice (Figure 2G). This resulted in a stepwise reduction in complex I-supported respiration (CI_P) at maximum ADP concentrations in muscles of *mdx* and *dko* mice (Figure 2C). Similar responses were also observed in complex II-supported respiration ($CI + II_P$) after LFS

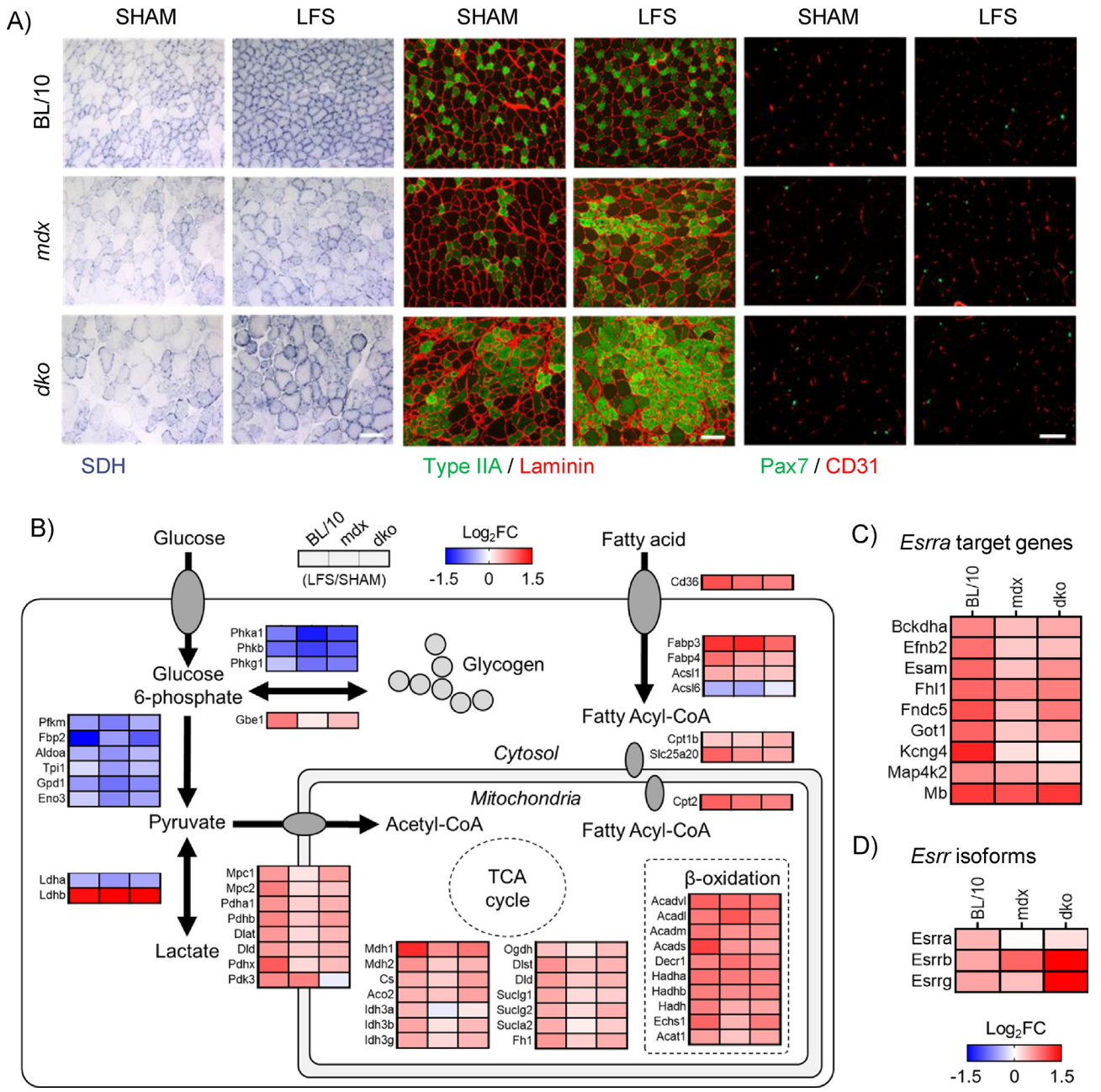

Figure 1: Loss of dystrophin and utrophin in dystrophic muscles impairs transcriptional remodeling to low-frequency stimulation (LFS). (A) Representative images of tibialis anterior (TA) muscle succinate dehydrogenase (SDH) enzyme activity (left panel; scale bar = 100 μm), myosin heavy-chain type IIA expression (middle panel; scale bar = 100 μm), and CD31+ endothelial cells and Pax7+ stem (satellite) cells (right panel; scale bar = 50 μm). (B) Expression of genes involved in glycolytic and fatty acid metabolism assessed by RNA sequencing in extensor digitorum longus (EDL) muscles (n = 3/group) increased by LFS in red, decreased by LFS in blue. (C) Expression of *Esrra* target genes assessed by RNA sequencing in EDL muscles (n = 3/group). (D) Expression of estrogen-related receptor isoforms assessed by RNA sequencing in EDL muscles (n = 3/group).

(Figure 2D). Collectively, these data suggest that loss of dystrophin in dystrophic muscles impairs adaptations to mitochondrial function after LFS, and loss of dystrophin and utrophin in dystrophic muscles promotes dyscoupling of mitochondrial content and function.

Although a role for utrophin in the regulation of mitochondrial homeostasis has been suggested from studies using transgenic and pharmacological approaches to increase utrophin expression in dystrophin-deficient muscles, the adaptive responses to physiological stimuli in the presence or absence of dystrophin and utrophin are not well understood. Chronic LFS reduced gastrocnemius muscle mass in wild-type mice (Figure S3A), with a concomitant increase in citrate synthase enzyme activity (Figure S3B). These adaptive responses were not altered in muscles of *mdx* and *dko* mice (Figure S3A,B), suggesting that the ability to increase mitochondrial content with contractile activity remained intact. To further elucidate a role for dystrophin and utrophin in mitochondrial homeostasis of dystrophic muscle, we performed proteomics on mitochondria mechanically isolated from gastrocnemius muscles and normalized by total protein. We detected a total of 469 known mitochondrial proteins across all conditions, with 307 being differentially expressed by LFS in at least one genotype ($p < 0.05$)

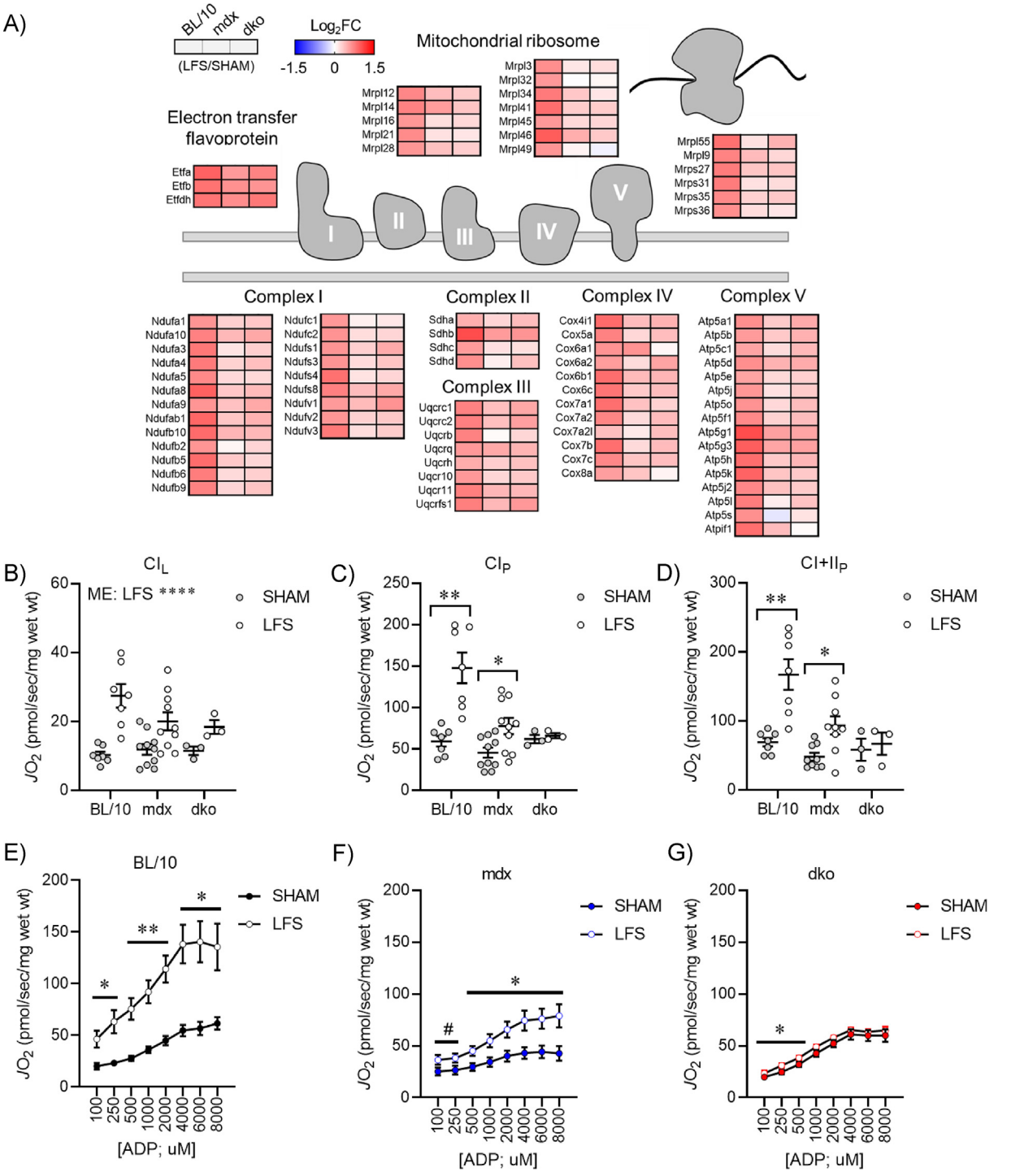

Figure 2: Loss of dystrophin and utrophin in dystrophic muscles impairs transcriptional remodeling of oxidative phosphorylation with low-frequency stimulation (LFS). (A) Expression of genes involved in oxidative phosphorylation and mitochondrial ribosomes assessed by RNA sequencing in extensor digitorum longus (EDL) muscles (n = 3/group) increased by LFS in red, decreased by LFS in blue. (B) Complex I-supported leak respiration (CI_L; pyruvate + malate) in permeabilized EDL fibers assessed by high-resolution respirometry (n = 3–10/group). (C) Complex I-supported coupled respiration (CI_P) in permeabilized EDL fibers assessed by high-resolution respirometry (n = 3–10/group). (D) Complex II-supported coupled respiration ($CI + II_P$) in permeabilized EDL fibers assessed by high-resolution respirometry (n = 3–10/group). (E–G) Complex I-supported respiration (CI_P; pyruvate + malate + ADP) at varying [ADP] (100–8,000 μM) in permeabilized EDL fibers of BL/10 (E), *mdx* (F), and *dko* (G) mice assessed by high-resolution respirometry (n = 3–10/group). Data are means ± SEM. Two-way ANOVA followed by Tukey's multiple comparison test (B–D); Paired Student's t-test (E–G); ME: main effect; #$p < 0.10$, *$p < 0.05$, **$p < 0.01$, ****$p < 0.0001$.

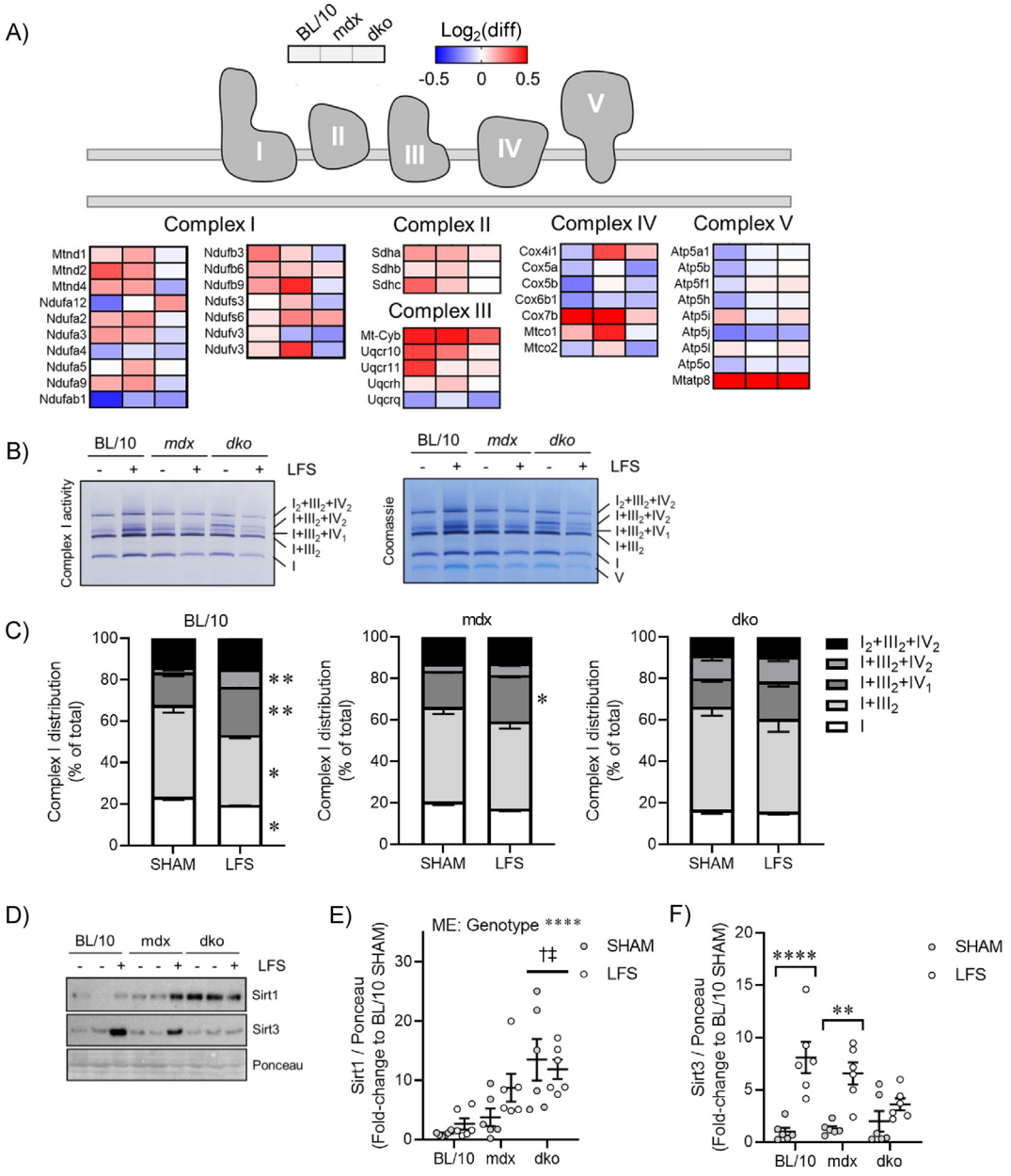

Figure 3: Loss of dystrophin and utrophin in dystrophic muscles impairs mitochondrial remodeling to low-frequency stimulation (LFS). (A) Expression of respiratory chain complexes assessed by mitochondrial proteomics in gastrocnemius (GAS) muscles (n = 3/group). (B) Representative image of complex I enzyme activity (native and supercomplexes) and total protein staining (Coomassie) assessed by blue native polyacrylamide gel electrophoresis (PAGE) in GAS muscles. (C) Percentage of mitochondrial complex I in native and supercomplexes assessed by blue native PAGE in GAS muscles (n = 6/group). (D) Representative image of Sirt1 and Sirt3 protein expression assessed by western blot in whole GAS muscle lysate. (E and F) Quantification of Sirt1 (E) and Sirt3 (F) protein expression assessed by western blot in whole GAS muscle lysate (n = 6/group). Data are means ± SEM; unpaired Student's t-test (C); two-way ANOVA followed by Tukey's multiple comparison test (E and F); ME: main effect; † difference to BL/10; ‡ difference to *mdx*; *p < 0.05, **p < 0.01, ****p < 0.0001.

(Figure S3C-F). Biological processes and Kyoto Encyclopedia of Genes and Genomes (KEGG) pathway terms related to the TCA cycle, NADH metabolic process, and carbon metabolism were overrepresented in proteins increased by LFS (Figure S3G), which was also observed in *mdx* and *dko* mice. Terms related to oxidative phosphorylation were not overrepresented in muscles of *dko* mice (Figure S3G), which was further supported by the absence of *Essra*-regulated proteins identified by transcription factor enrichment analyses (Figure S3H).

We observed a preferential increase in the expression of subunits belonging to complexes I, II, and III after LFS in muscles of wild-type and *mdx* mice (Figure 3A), which was abrogated in muscles of *dko* mice. Enhanced respiratory capacity after endurance exercise training is accompanied by remodeling of native complex I into supramolecular weight complexes, known as supercomplexes [43]. While the functional significance of supercomplexes is not entirely clear, this dynamic remodeling process may facilitate enhanced respiratory chain efficiency and reduced oxidative damage in response to cellular perturbations (reviewed in [44]). Strikingly, we observed a redistribution of native and supercomplexes containing complexes I and III (e.g., I and I + III_2) to higher molecular weight complexes containing I + III_n + IV_n

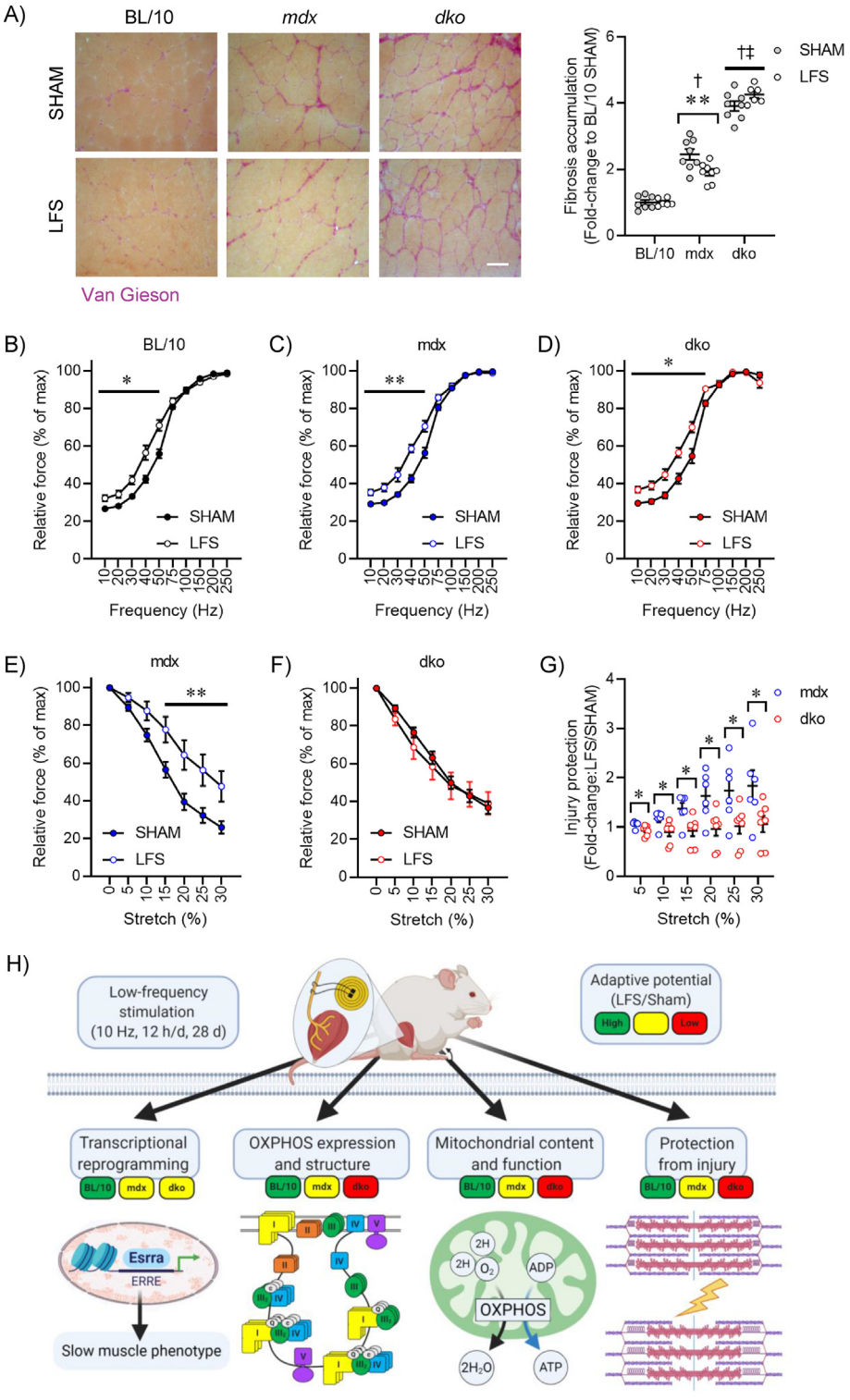

Figure 4: Loss of utrophin in dystrophin-deficient muscles impairs adaptive remodeling and protection from contraction-induced injury after low-frequency stimulation (LFS). (A) Representative tibialis anterior (TA) muscle fibrosis staining (*left*) and quantification (*right*) (n = 6–8/group). Scale bar = 50 μm. (B–D) Relative tetanic force production (% of maximal) of TA muscles (*in situ*) at various stimulation frequencies in BL/10 (B), *mdx* (C), and *dko* (D) mice (n = 6–16/group). (E and F) Eccentric contraction-induced injury in TA muscles (*in situ*) of *mdx* (E) and *dko* (F) mice (n = 6–16/group). (G) Degree of protection during TA eccentric contraction-induced injury (n = 6–7/group). (H) Summary describing the role of dystrophin and utrophin in metabolic and contractile remodeling with LFS. Created with BioRender.com. Data are means ± SEM; two-way ANOVA followed by Tukey's multiple comparison test (A); † difference to BL/10; ‡ difference to *mdx*; unpaired Student's t-test (B–G); *p < 0.05, **p < 0.01.

and I_2+III_2+IV_2 with LFS in muscles of wild-type mice (Figure 3B,C). While this redistribution was also observed to a lesser extent in muscles of *mdx* mice, this remodeling did not occur in muscles of *dko* mice (Figure 3B,C). Interestingly, we observed an increase in both complex I enzyme activity and total abundance in mitochondria of wild-type mice with LFS (Figure 3B). Since this analysis was normalized to mitochondrial protein content (e.g., μg protein), it implies that LFS increased the abundance of both native and supercomplexes in mitochondria. Together, these results suggest that LFS increases muscle mitochondrial content, the expression of subunits belonging to complexes I-III within mitochondria, and the redistribution of the respiratory chain into supercomplexes. This remodeling is impaired in dystrophin-deficient muscles and completely abrogated by the loss of dystrophin and utrophin in dystrophic muscles.

Sirtuin 1 (Sirt1) and sirtuin 3 (Sirt3) have been implicated in linking contractile-induced metabolic perturbations to transcriptional reprogramming of metabolism, mitochondrial biogenesis, and respiratory function through modulating activity of the transcriptional coactivator peroxisome proliferator-activated receptor gamma coactivator 1-alpha (*Ppargc1a*), which interacts with *Esrra* [26,45]. We found differential expression of Sirt1 and Sirt3 in response to dystrophic pathology and LFS. Basal Sirt1 expression was increased significantly in muscles of *dko* mice (Figure 3D,E), suggesting a dysregulation of mitochondrial content, structure, and function with the loss of utrophin in dystrophic muscle. While Sirt3 expression was highly responsive to LFS in muscles of wild-type and *mdx* mice (Figure 3D,F), this sensitivity was disrupted in muscles of *dko* mice (Figure 3F). Overall, these data provide novel evidence that the proteomic remodeling of oxidative phosphorylation with LFS is disrupted by the loss of dystrophin and utrophin in dystrophic muscles, which is linked to perturbed cell signaling and transcriptional regulation of cellular metabolism. In fact, the dyscoupling of mitochondrial function, cell signaling, and transcription in muscles of *dko* mice suggests the accumulation of dysfunctional mitochondria.

Loss of dystrophin renders fast, glycolytic fibers susceptible to wasting and dysfunction [1], and the possibility exists that high mechanical forces applied during exercise and/or through stimulated contractions may be contraindicative to treatment goals. We provide convincing evidence that LFS does not increase central nucleation, CD68+ inflammatory cells, or immunoglobulin G (IgG) accumulation in TA muscles of *mdx* and *dko* mice (Figure S4A-D). Further, we found that LFS reduced fibrosis in *mdx* mice, which was dependent on the presence of utrophin expression in dystrophic muscles (Figure 4A). Given that fibrosis is often linked to disrupted functional capacity, we then evaluated whether TA muscle function *in situ* (with nerve and blood supply intact) was improved after LFS. The leftward shift in the frequency—force relationship, indicative of slow-like adaptations in contractility, was similar in muscles of *mdx* and *dko* mice (Figure 4B—D). This contractile remodeling after LFS was consistent with reductions in absolute tetanic force, with these effects most prominent in muscles of *mdx* and *dko* mice (Figure S5A-D). Specific force was minimally affected after LFS, indicating preservation of the intrinsic force-generating capacity of dystrophic muscles (Figure S5E). These changes in contractile kinetics were supported by increased expression of slow myosin heavy-chain and Ca^{2+} handling genes in EDL muscles of wild-type and dystrophic mice (Figure S5F).

Although utrophin has been implicated in mediating functional protection during slow muscle remodeling, no studies have clearly defined biological roles of dystrophin and utrophin in dystrophic muscle adaptation and plasticity to LFS. It was clinically relevant to determine whether LFS could confer protection to muscles from contraction-mediated injury. To this end, TA muscles (*in situ*) were subjected to repeated bouts of eccentric contractions at maximal stimulation and with progressive increments of stretch to cause cumulative damage [42]. Dystrophic muscles produced less isometric force after each eccentric contraction, whereas LFS attenuated this loss of force in muscles of *mdx* mice (Figure 4E). In contrast, the protection conferred by LFS was abrogated in muscles of *dko* mice (Figure 4F), with the greatest improvements in protection observed at higher levels of stretch in muscles of *mdx* mice (Figure 4G). Overall, these findings demonstrate that loss of utrophin in dystrophic muscles impairs adaptive remodeling and protection from contraction-induced injury after LFS.

In summary, we revealed novel biological roles of dystrophin and utrophin in the adaptation and plasticity of dystrophic muscle to chronic LFS, involving transcriptional reprogramming, remodeling of the mitochondrial proteome and respiratory chain supercomplexes, enhanced fiber respiration, and protection from contraction-induced injury (Figure 4G). Future experiments combining LFS with gene and/or cell therapies to restore dystrophin/utrophin expression will help to define their specific roles in this impaired metabolic remodeling. The current findings provide mechanistic bases for optimizing efficacious LFS protocols for potential therapeutic application in DMD and related muscle disorders.

AUTHOR CONTRIBUTIONS

Justin P. Hardee: investigation, formal analysis, data curation, validation, visualization, project administration, funding acquisition, writing — original draft, writing — review and editing; **Karen J.B. Martins:** conceptualization, methodology, investigation, formal analysis, project administration, writing — review and editing; **Paula M. Miotto:** formal analysis, investigation, writing — review and editing; **James G. Ryall:** data curation, investigation, formal analysis, writing — review and editing; **Stefan M. Gehrig:** formal analysis, investigation; **Boris Reljic:** formal analysis, investigation, funding acquisition, writing — review and editing; **Timur Naim:** formal analysis, investigation; **Dylan J. Chung:** formal analysis, investigation, writing — review and editing; **Jen Trieu:** formal analysis, investigation; **Kristy Swiderski:** formal analysis, investigation, writing — review and editing; **Ashleigh M. Philp:** formal analysis, investigation; **Andrew Philp:** resources, supervision, writing — review and editing; **Matthew J. Watt:** resources, supervision, writing — review and editing; **David A. Stroud:** resources, supervision, funding acquisition, writing — review and editing; **Rene Koopman:** resources, writing — review and editing; **Gregory R. Steinberg:** Funding acquisition, writing — review and editing; **Gordon S. Lynch:** conceptualization, formal analysis, project administration, supervision, funding acquisition, writing — original draft, writing — review and editing.

ACKNOWLEDGMENTS

We gratefully acknowledge the assistance and advice from Dr. Charles T. Putman, Dr. Kelvin E. Jones, and Zoltan Kenwell (electronics specialist) from the University of Alberta when establishing the wireless stimulator model with K.J.M. during the development phase of the project. J.P.H was supported by a McKenzie Research Fellowship from The University of Melbourne. P.M.M was supported by a Natural Sciences and Engineering Research Council of Canada (NSERC) Post-Doctoral Fellowship. This work was supported by research grants from the National Health and Medical Research Council (GNT1124474; GNT1140906; GNT1140851), The University of Melbourne's School of Biomedical Sciences Early-Mid Career Research Association (EMCRA) Collaborative Award, and The University of Melbourne's Medicine, Dentistry, and Health Sciences Large Equipment Grant Scheme. We thank the Bio21 Mass Spectrometry and Proteomics Facility (MMSPF) for the provision of instrumentation, training, and technical support.

CONFLICT OF INTEREST

None declared.

APPENDIX A. SUPPLEMENTARY DATA

Supplementary data to this article can be found online at https://doi.org/10.1016/j.molmet.2020.101157.

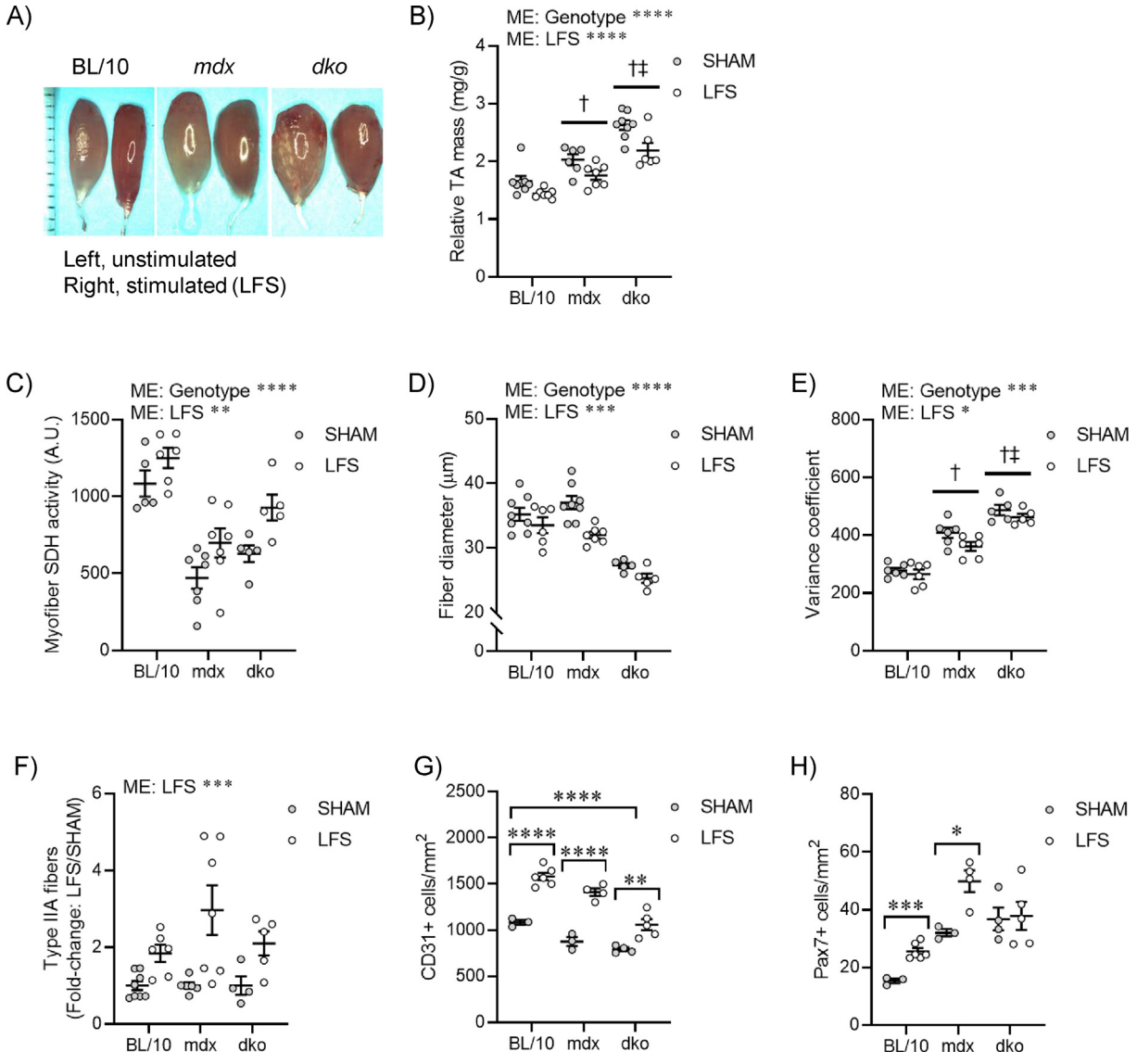

Figure S1: Morphological adaptations to low-frequency stimulation (LFS) are not impaired in dystrophic muscles. (A) Gross appearance of tibialis anterior (TA) muscles. (B) Relative TA muscle mass (n = 6–8/group). (C) TA myofiber succinate dehydrogenase (SDH) enzyme activity (n = 4–7/group). (D) TA myofiber diameter (n = 5–6/group). (E) TA variance coefficient (n = 5–6/group). (F) Fold induction (LFS/SHAM) of myosin heavy-chain type IIA fibers (n = 4–8/group). (G and H) CD31+ endothelial cell (G) and Pax7+ stem (satellite) cell (H) abundance in TA muscles (n = 3–6/group). Data are means ± SEM; two-way ANOVA followed by Tukey's multiple comparison test (B–H); ME: main effect; † difference to BL/10; ‡ difference to *mdx*; *p < 0.05, **p < 0.01, ***p < 0.001, ****p < 0.0001.

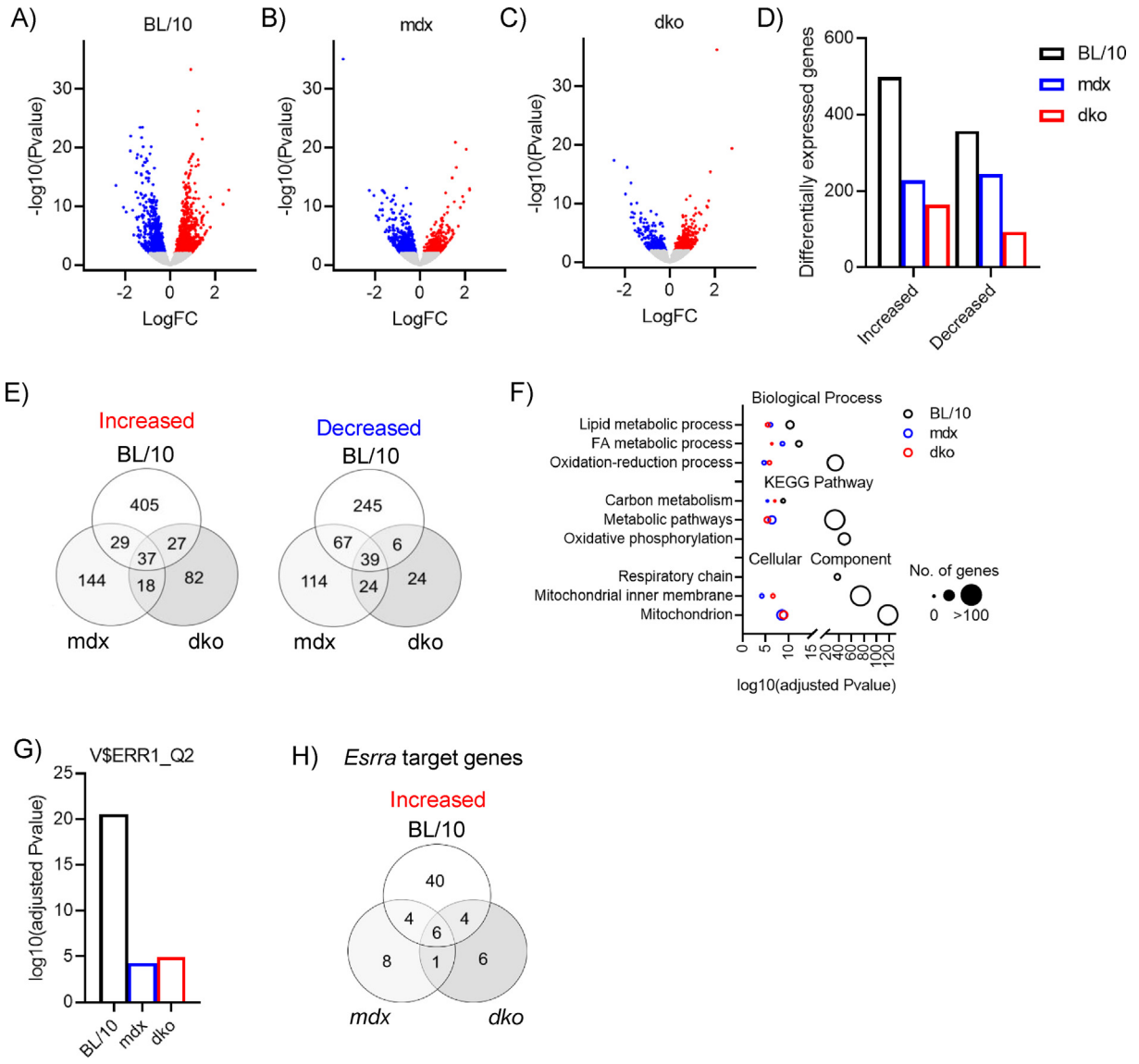

Figure S2: Loss of dystrophin and utrophin in dystrophic muscles impairs transcriptional remodeling to low-frequency stimulation (LFS). (A-C) Volcano plot of differentially expressed genes in BL/10 (A), *mdx* (B), and *dko* (C) mice assessed by RNA sequencing in extensor digitorum longus (EDL) muscles increased by LFS in red, decreased by LFS in blue (n = 3/group). (D) Total number of genes increased or decreased by LFS assessed by RNA sequencing in EDL muscles (n = 3/group). (E) Venn diagram of the number of differentially expressed genes increased or decreased by LFS assessed by RNA sequencing in EDL muscles (n = 3/group). (F) Gene set enrichment analysis of genes increased by LFS assessed by RNA sequencing in EDL muscles; number of genes in each category is indicated by the size of circle (n = 3/group). (G) Identification of estrogen-related receptor alpha (*Esrra*) by transcription factor enrichment analysis of genes increased by LFS in EDL muscles (n = 3/group). (H) Venn diagram of the number of *Esrra* target genes increased by LFS in EDL muscles (n = 3/group).

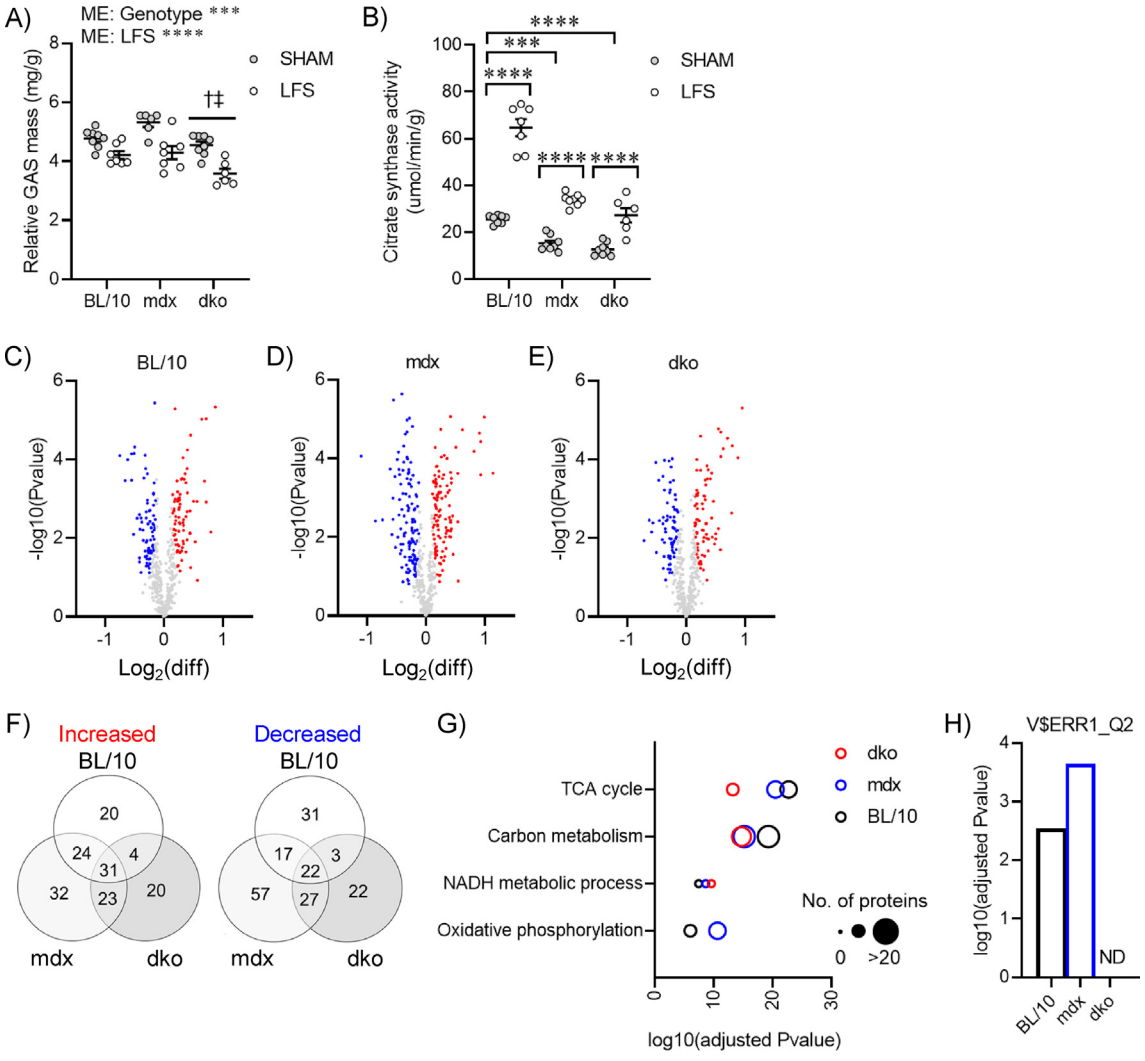

Figure S3: Loss of dystrophin and utrophin in dystrophic muscles disrupts remodeling of the mitochondrial proteome with low-frequency stimulation (LFS). (A) Relative gastrocnemius (GAS) muscle mass (n = 6–8/group). (B) Citrate synthase enzyme activity in whole GAS muscle lysate (n = 6–8/group). (C-E) Volcano plot of differentially expressed proteins in BL/10 (C), *mdx* (D), and *dko* (E) mice assessed by mitochondrial proteomics in GAS muscles increased by LFS in red, decreased by LFS in blue (n = 3/group). (F) Venn diagram of the number of differentially expressed proteins increased or decreased by LFS assessed by mitochondrial proteomics in GAS muscles (n = 3/group). (G) Gene set enrichment analysis of proteins increased by LFS assessed by mitochondrial proteomics in GAS muscles (n = 3/group). (H) Identification of estrogen-related receptor alpha (Esrra) by transcription factor enrichment analysis of proteins increased by LFS in GAS muscles (n = 3/group). Data are means ± SEM; two-way ANOVA followed by Tukey's multiple comparison test (A and B); ME: main effect; † difference to BL/10; ‡ difference to *mdx*; ***$p < 0.001$, ****$p < 0.0001$.

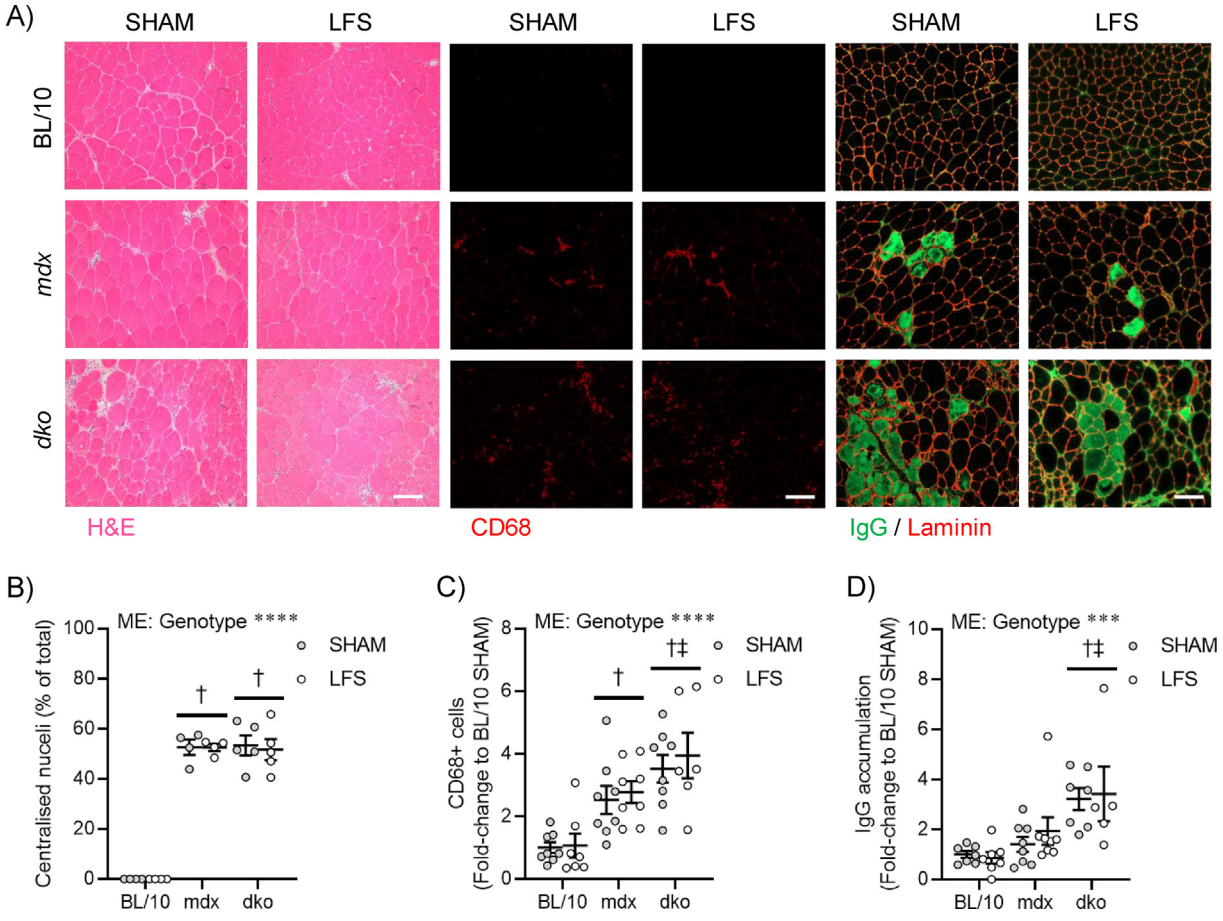

Figure S4: Aspects of the dystrophic pathology are not aggravated by low-frequency electrical stimulation (LFS). (A) Representative tibialis anterior (TA) histological images for general morphology (hematoxylin and eosin, H&E; left; scale bar = 50 μm), CD68+ inflammatory cells (middle; scale bar = 50 μm) and immunoglobulin G (IgG) accumulation (right; scale bar = 50 μm). (B-D) Quantification of centralized nuclei (B), CD68+ inflammatory cells (C), and IgG accumulation (D) after LFS in TA muscles (n = 4–5/group). Data are means ± SEM; two-way ANOVA followed by Tukey's multiple comparison test (B-D); ME: main effect; † difference to BL/10; ‡ difference to *mdx*; ***$p < 0.001$, ****$p < 0.0001$.

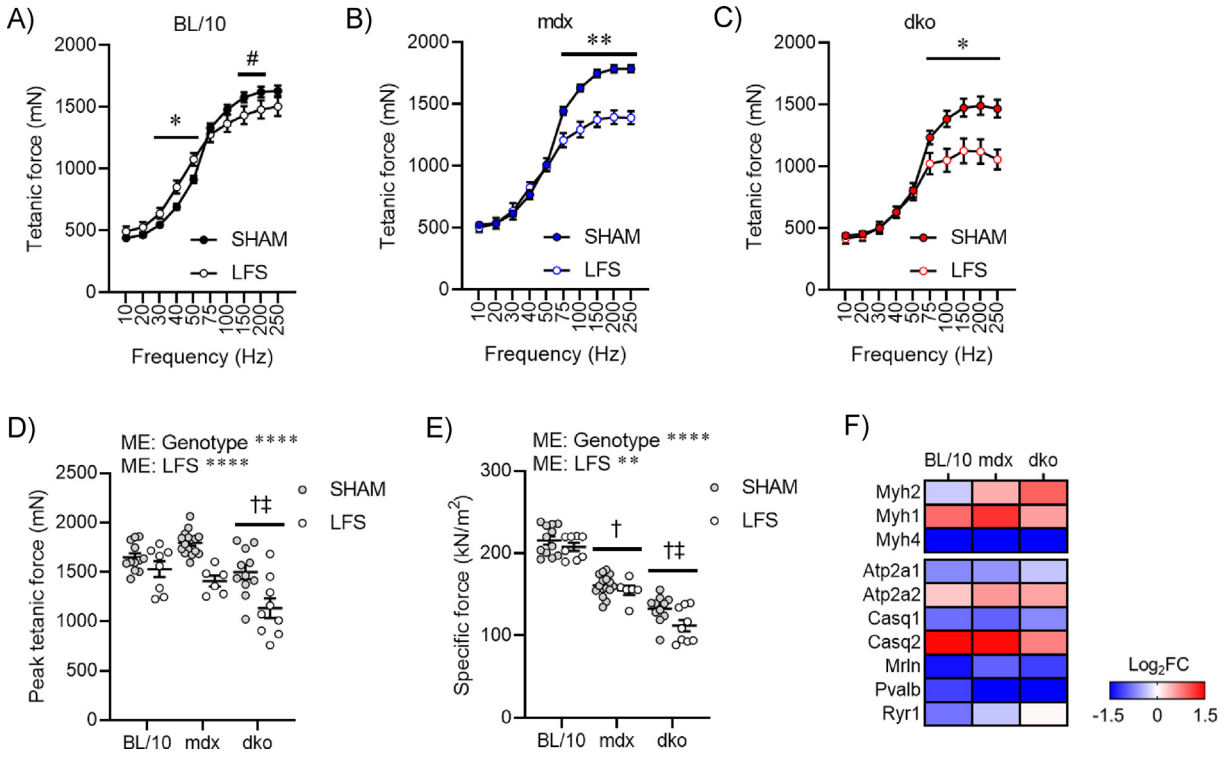

Figure S5: Contractile remodeling to LFS is not impaired in dystrophic muscle. (A-C) Tetanic force production of tibialis anterior (TA) muscles at various stimulation frequencies in BL/10 (A), *mdx* (B), and *dko* (C) mice assessed *in situ* (n = 6–16/group). (D and E) Peak (D) and specific (E) force of TA muscles (*in situ*) at maximal stimulation (n = 6–16/group). (F) Expression of genes involved in contraction and calcium handling assessed by RNA sequencing in EDL muscles (n = 3/group), increased by LFS in red, decreased by LFS in blue. Data are means ± SEM; Student's t-test (A-C); two-way ANOVA followed by Tukey's multiple comparison test (D and E); ME: main effect; † difference to BL/10; ‡ difference to *mdx*; #p < 0.10, *p < 0.05, **p < 0.01, ****p < 0.0001.

REFERENCES

[1] Webster, C., Silberstein, L., Hays, A.P., Blau, H.M., 1988. Fast muscle fibers are preferentially affected in Duchenne muscular dystrophy. Cell 52(4):503–513.

[2] Gramolini, A.O., Belanger, G., Thompson, J.M., Chakkalakal, J.V., Jasmin, B.J., 2001. Increased expression of utrophin in a slow vs. a fast muscle involves posttranscriptional events. American Journal of Physiology - Cell Physiology 281(4):C1300–C1309.

[3] Chakkalakal, J.V., Stocksley, M.A., Harrison, M.A., Angus, L.M., Deschenes-Furry, J., St-Pierre, S., et al., 2003. Expression of utrophin A mRNA correlates with the oxidative capacity of skeletal muscle fiber types and is regulated by calcineurin/NFAT signaling. Proceedings of the National Academy of Sciences of the United States of America 100(13):7791–7796.

[4] Deconinck, N., Tinsley, J., De Backer, F., Fisher, R., Kahn, D., Phelps, S., et al., 1997. Expression of truncated utrophin leads to major functional improvements in dystrophin-deficient muscles of mice. Nature Medicine 3(11):1216–1221.

[5] Gilbert, R., Nalbanoglu, J., Tinsley, J.M., Massie, B., Davies, K.E., Karpati, G., 1998. Efficient utrophin expression following adenovirus gene transfer in dystrophic muscle. Biochemical and Biophysical Research Communications 242(1):244–247.

[6] Tinsley, J.M., Potter, A.C., Phelps, S.R., Fisher, R., Trickett, J.I., Davies, K.E., 1996. Amelioration of the dystrophic phenotype of mdx mice using a truncated utrophin transgene. Nature 384(6607):349–353.

[7] Lynch, G.S., 2017. Therapeutic potential of skeletal muscle plasticity and slow muscle programming for muscular dystrophy and related muscle conditions. In: Sakuma, K. (Ed.), The plasticity of skeletal muscle: from molecular mechanism to clinical applications. Singapore: Springer Singapore. p. 277–92.

[8] Ljubicic, V., Burt, M., Jasmin, B.J., 2014. The therapeutic potential of skeletal muscle plasticity in Duchenne muscular dystrophy: phenotypic modifiers as pharmacologic targets. The FASEB Journal 28(2):548–568.

[9] Capitanio, D., Moriggi, M., Torretta, E., Barbacini, P., De Palma, S., Vigano, A., et al., 2020. Comparative proteomic analyses of Duchenne muscular dystrophy and Becker muscular dystrophy muscles: changes contributing to preserve muscle function in Becker muscular dystrophy patients. Journal Cachexia Sarcopenia Muscle 11(2):547–563.

[10] Gaglianone, R.B., Santos, A.T., Bloise, F.F., Ortiga-Carvalho, T.M., Costa, M.L., Quirico-Santos, T., et al., 2019. Reduced mitochondrial respiration and increased calcium deposits in the EDL muscle, but not in soleus, from 12-week-old dystrophic mdx mice. Scientific Reports 9(1):1986.

[11] Hughes, M.C., Ramos, S.V., Turnbull, P.C., Rebalka, I.A., Cao, A., Monaco, C.M.F., et al., 2019. Early myopathy in Duchenne muscular dystrophy is associated with elevated mitochondrial H2 O2 emission during impaired oxidative phosphorylation. Journal Cachexia Sarcopenia Muscle 10(3):643–661.

[12] Pette, D., Heilig, A., Klug, G., Reichmann, H., Seedorf, U., Wiehrer, W., 1985. Alterations in phenotype expression of muscle by chronic nerve stimulation. Advances in Experimental Medicine & Biology 182:169–177.

[13] Pette, D., Smith, M.E., Staudte, H.W., Vrbova, G., 1973. Effects of long-term electrical stimulation on some contractile and metabolic characteristics of fast rabbit muscles. Pflügers Archiv 338(3):257–272.

[14] Scott, O.M., Vrbova, G., Hyde, S.A., Dubowitz, V., 1986. Responses of muscles of patients with Duchenne muscular dystrophy to chronic electrical stimulation. Journal of Neurology Neurosurgery and Psychiatry 49(12):1427–1434.

[15] Zupan, A., 1992. Long-term electrical stimulation of muscles in children with Duchenne and Becker muscular dystrophy. Muscle & Nerve 15(3):362–367.

[16] Zupan, A., Gregorič, M., Valenčic, V., 1995. Long-lasting effects of electrical stimulation upon muscles of patients suffering from progressive muscular dystrophy. Clinical Rehabilitation 9(2):102—109.
[17] Zupan, A., Gregoric, M., Valencic, V., Vandot, S., 1993. Effects of electrical stimulation on muscles of children with Duchenne and Becker muscular dystrophy. Neuropediatrics 24(4):189—192.
[18] Dangain, J., Vrbova, G., 1989. Long term effect of low frequency chronic electrical stimulation on the fast hind limb muscles of dystrophic mice. Journal of Neurology Neurosurgery and Psychiatry 52(12):1382—1389.
[19] Luthert, P., Vrbova, G., Ward, K.M., 1980. Effects of slow frequency electrical stimulation on muscles of dystrophic mice. Journal of Neurology Neurosurgery and Psychiatry 43(9):803—809.
[20] Vrbova, G., Ward, K., 1981. Observations on the effects of low frequency electrical stimulation on fast muscles of dystrophic mice. Journal of Neurology Neurosurgery and Psychiatry 44(11):1002—1006.
[21] McGreevy, J.W., Hakim, C.H., McIntosh, M.A., Duan, D., 2015. Animal models of Duchenne muscular dystrophy: from basic mechanisms to gene therapy. Disease Model Mechanics 8(3):195—213.
[22] Deconinck, A.E., Rafael, J.A., Skinner, J.A., Brown, S.C., Potter, A.C., Metzinger, L., et al., 1997. Utrophin-dystrophin-deficient mice as a model for Duchenne muscular dystrophy. Cell 90(4):717—727.
[23] Gehrig, S.M., van der Poel, C., Sayer, T.A., Schertzer, J.D., Henstridge, D.C., Church, J.E., et al., 2012. Hsp72 preserves muscle function and slows progression of severe muscular dystrophy. Nature 484(7394):394—398.
[24] Murphy, K.T., Allen, A.M., Chee, A., Naim, T., Lynch, G.S., 2012. Disruption of muscle renin-angiotensin system in AT1a-/- mice enhances muscle function despite reducing muscle mass but compromises repair after injury. American Journal of Physiology - Regulatory, Integrative and Comparative Physiology 303(3):R321—R331.
[25] Schertzer, J.D., Gehrig, S.M., Ryall, J.G., Lynch, G.S., 2007. Modulation of insulin-like growth factor (IGF)-I and IGF-binding protein interactions enhances skeletal muscle regeneration and ameliorates the dystrophic pathology in mdx mice. American Journal Of Pathology 171(4):1180—1188.
[26] Ryall, J.G., Dell'Orso, S., Derfoul, A., Juan, A., Zare, H., Feng, X., et al., 2015. The NAD(+)-dependent SIRT1 deacetylase translates a metabolic switch into regulatory epigenetics in skeletal muscle stem cells. Cell Stem Cell 16(2):171—183.
[27] Afgan, E., Baker, D., van den Beek, M., Blankenberg, D., Bouvier, D., Cech, M., et al., 2016. The Galaxy platform for accessible, reproducible and collaborative biomedical analyses: 2016 update. Nucleic Acids Research 44(W1). W3-W10.
[28] Kim, D., Pertea, G., Trapnell, C., Pimentel, H., Kelley, R., Salzberg, S.L., 2013. TopHat2: accurate alignment of transcriptomes in the presence of insertions, deletions and gene fusions. Genome Biology 14(4):R36.
[29] Trapnell, C., Pachter, L., Salzberg, S.L., 2009. TopHat: discovering splice junctions with RNA-Seq. Bioinformatics 25(9):1105—1111.
[30] Huang da, W., Sherman, B.T., Lempicki, R.A., 2009. Systematic and integrative analysis of large gene lists using DAVID bioinformatics resources. Nature Protocols 4(1):44—57.
[31] Subramanian, A., Tamayo, P., Mootha, V.K., Mukherjee, S., Ebert, B.L., Gillette, M.A., et al., 2005. Gene set enrichment analysis: a knowledge-based approach for interpreting genome-wide expression profiles. Proceedings of the National Academy of Sciences of the United States of America 102(43): 15545—15550.
[32] Liberzon, A., Subramanian, A., Pinchback, R., Thorvaldsdottir, H., Tamayo, P., Mesirov, J.P., 2011. Molecular signatures database (MSigDB) 3.0. Bioinformatics 27(12):1739—1740.
[33] Doerrier, C., Garcia-Souza, L.F., Krumschnabel, G., Wohlfarter, Y., Meszaros, A.T., Gnaiger, E., 2018. High-resolution FluoRespirometry and OXPHOS protocols for human cells, permeabilized fibers from small biopsies of muscle, and isolated mitochondria. Methods in Molecular Biology 1782:31—70.
[34] Miotto, P.M., McGlory, C., Bahniwal, R., Kamal, M., Phillips, S.M., Holloway, G.P., 2019. Supplementation with dietary omega-3 mitigates immobilization-induced reductions in skeletal muscle mitochondrial respiration in young women. The FASEB Journal 33(7):8232—8240.
[35] Jha, P., Wang, X., Auwerx, J., 2016. Analysis of mitochondrial respiratory chain supercomplexes using blue native polyacrylamide gel electrophoresis (BN-PAGE). Current Protocols in Mouse Biology 6(1):1—14.
[36] Stroud, D.A., Surgenor, E.E., Formosa, L.E., Reljic, B., Frazier, A.E., Dibley, M.G., et al., 2016. Accessory subunits are integral for assembly and function of human mitochondrial complex I. Nature 538(7623):123—126.
[37] Dibley, M.G., Formosa, L.E., Lyu, B., Reljic, B., McGann, D., Muellner-Wong, L., et al., 2020. The mitochondrial acyl-carrier protein interaction network highlights important roles for LYRM family members in complex I and mitoribosome assembly. Molecular & Cellular Proteomics 19(1):65—77.
[38] Cox, J., Mann, M., 2008. MaxQuant enables high peptide identification rates, individualized p.p.b.-range mass accuracies and proteome-wide protein quantification. Nature Biotechnology 26(12):1367—1372.
[39] Tyanova, S., Temu, T., Sinitcyn, P., Carlson, A., Hein, M.Y., Geiger, T., et al., 2016. The Perseus computational platform for comprehensive analysis of (prote)omics data. Nature Methods 13(9):731—740.
[40] Calvo, S.E., Clauser, K.R., Mootha, V.K., 2016. MitoCarta2.0: an updated inventory of mammalian mitochondrial proteins. Nucleic Acids Research 44(D1): D1251—D1257.
[41] Joanisse, S., Ashcroft, S., Wilkinson, D.J., Pollock, R.D., O'Brien, K.A., Phillips, B.E., et al., 2020. High levels of physical activity in later life are associated with enhanced markers of mitochondrial metabolism. Journals of Gerontology Series A: Biological and Medical Sciences 75(8):1481—1487.
[42] Gehrig, S.M., Koopman, R., Naim, T., Tjoakarfa, C., Lynch, G.S., 2010. Making fast-twitch dystrophic muscles bigger protects them from contraction injury and attenuates the dystrophic pathology. American Journal Of Pathology 176(1):29—33.
[43] Greggio, C., Jha, P., Kulkarni, S.S., Lagarrigue, S., Broskey, N.T., Boutant, M., et al., 2017. Enhanced respiratory chain supercomplex formation in response to exercise in human skeletal muscle. Cell Metabolism 25(2):301—311.
[44] Hirst, J., 2018. Open questions: respiratory chain supercomplexes-why are they there and what do they do? BMC Biology 16(1):111.
[45] Philp, A., Schenk, S., 2013. Unraveling the complexities of SIRT1-mediated mitochondrial regulation in skeletal muscle. Exercise and Sport Sciences Reviews 41(3):174—181.

